

A Coupled Dynamical and Chemical Model of Starless Cores of Magnetized Molecular Clouds: I. Formulation and Initial Results

Zhi-Yun Li

Department of Astronomy, University of Virginia, P.O. Box 3818, Charlottesville, VA 22903

and

V. I. Shematovich, D. S. Wiebe and B. M. Shustov

Institute of Astronomy of the RAS, 48, Pyatnitskaya str., 109017 Moscow, Russia

ABSTRACT

We develop a detailed chemical model for the starless cores of strongly magnetized molecular clouds, with the ambipolar diffusion-driven dynamic evolution of the clouds coupled to the chemistry through ion abundances. We concentrate on two representative model clouds in this initial study, one with magnetic fields and the other without. The model predictions on the peak values and spatial distributions of the column densities of CO, CCS, N₂H⁺ and HCO⁺ are compared with those observationally inferred for the well-studied starless core L1544, which is thought to be on the verge of star formation. We find that the magnetic model, in which the cloud is magnetically supported for several million years before collapsing dynamically, provides a reasonable overall fit to the available data on L1544; the fit is significantly worse for the non-magnetic model, in which the cloud collapses promptly. The observed large peak column density for N₂H⁺ and clear central depression for CCS favor the magnetically-retarded collapse over the free-fall collapse. A relatively high abundance of CCS is found in the magnetic model, resulting most likely from an interplay of depletion and late-time hydrocarbon chemistry enhanced by CO depletion. These initial results lend some support to the standard picture of dense core formation in strongly magnetized clouds through ambipolar diffusion. They are at variance with those of Aikawa et al. (2001) who considered a set of models somewhat different from ours and preferred one in which the cloud collapses more or less freely for L1544.

Subject headings: ISM: clouds - ISM: individual (L1544) - ISM: molecules - ISM: magnetic fields - MHD - stars: formation

1. Introduction

Through a close interplay between theory and observation, a “standard” picture for the formation of isolated, low-mass stars has emerged (Shu, Adams & Lizano 1987). At the heart of this

picture lie the so-called “dense cores”, studied extensively by Myers and coworkers (e.g., Myers 1999). These dense cores are intimately associated with star formation, with roughly half of them already harboring infrared sources (Beichman et al. 1986). The other half are termed “starless cores”, and they are the focus of our investigation.

The starless cores are thought to be condensed out of strongly magnetized, turbulent background clouds. Direct Zeeman measurements to date, as compiled by Crutcher (1999), suggest that the field strength is close to the critical value required for the molecular cloud support, after likely geometric corrections (Shu et al. 1999). Core formation can be driven by either turbulence decay (Myers 1999) or ambipolar diffusion. We shall focus on the latter, which has been studied quantitatively by many authors (e.g., Nakano 1979; Lizano & Shu 1989; Basu & Mouschovias 1994; Ciolek & Mouschovias 1994). A general conclusion is that dense cores are formed on a time scale several times the free fall time of the background. This relatively long formation time should leave a strong imprint on the chemistry of the cores.

The goal of our investigation is to predict the spatial distributions of various molecular species at different stages of cloud evolution. For this initial study, we will concentrate on CO, CS, CCS, NH₃, N₂H⁺ and HCO⁺, which are often used to probe the physical conditions of star-forming clouds. We take into account the feedback of chemistry on the cloud dynamics, through ion abundances, which regulate the ambipolar diffusion and thus cloud contraction rate. Through a detailed comparison of the predicted and observed chemical abundances of starless cores, we seek to provide further support for the standard picture of isolated star formation involving ambipolar diffusion. A starless core well suited for such a purpose is the dense core of L1544, for which an extensive data set is becoming available (e.g., Caselli et al. 2001a,b).

The L1544 starless core is located in the eastern part of the Taurus molecular cloud complex, at an estimated distance of 140 pc (Elias 1978). It is an elongated core that shows substantial infall motions (up to $\sim 0.1 \text{ km s}^{-1}$) on both large ($\sim 0.1 \text{ pc}$) and small ($\sim 0.01 \text{ pc}$) scales, based on single-disk observations of CO, ¹³CO, C¹⁸O, CS, C³⁴S, HCO⁺, and N₂H⁺ (Tafalla et al. 1998) and interferometric observations of N₂H⁺ (Williams et al. 1999). Interferometric observations of CCS by Ohashi et al. (1999) reveal a ring-like structure, which shows evidence for collapse as well as rotation. The low central emission is most likely due to a depletion of CCS, judging from the fact that dust continuum peaks inside the ring (Ward-Thompson, Motte & Andre 1999). Indeed, the column density distribution of the L1544 core is rather well determined¹, not only from the dust continuum emission, but also from absorption against a mid-infrared background (Bacmann et al. 2000). The core has a small, high column (and volume) density central plateau (of radius $\sim 2900 \text{ AU}$), surrounded by an envelope in which the column (and volume) density decreases rapidly outward, before it joins rather abruptly with the background at a radius of order 10^4 AU (Bacmann et al. 2000). The plateau-envelope structure has been interpreted in terms

¹See, however, Evans et al. (2001) who find that a singular isothermal sphere cannot be ruled out from the modeling of SCUBA data alone, when the lower temperature at the core center relative to edge is taken into account.

of the ambipolar diffusion-driven dynamical evolution of a magnetized cloud (Li 1999; Ciolek & Basu 2000), and the large column density contrast between the central plateau and the background (~ 20 ; Bacmann et al. 2000) suggests that the L1544 core is rather evolved (Williams et al. 1999), and may be on the verge of forming a star (or stellar system). Further evidence for the core being in an advanced stage of evolution comes from IRAM 30m observations of Caselli et al. (1999), who found that CO is depleted by a factor of order ~ 10 at the dust continuum peak. These authors also noted that the (likely) optically thin lines of $D^{13}CO^+$ and $HC^{18}O^+$ are double-peaked, which may be another indication that these species are centrally depleted and their emission comes mainly from an infalling *shell*. The wealth of molecular line and dust continuum data, coupled with the recent Zeeman measurement of magnetic field strength (Crutcher & Troland 2000) and the determination of magnetic field direction from submillimeter polarization measurements (Ward-Thompson et al. 2000), makes L1544 a Rosette Stone for theories of dense core condensation leading to isolated low-mass star formation.

Many of the dynamical and chemical features of L1544 are shared by L1498, another quiescent, elongated starless core also located in the Taurus molecular complex. Lemme et al. (1995) studied the core in detail, and found that the distributions of both $C^{18}O$ and CS are ring-like, indicating a central depletion of these two species. The CO depletion factor is inferred to be of order ~ 8 or higher (Willacy, Langer & Velusamy 1998), comparable to that of L1544, based on ISOPHOT 100 and 200 μm observations. Single-dish and interferometric observations of CCS (Kuiper, Langer & Velusamy 1996) show that its distribution is also ring-like. Moreover, the NH_3 emission appears to be centrally peaked, again similar to L1544. Perhaps most strikingly, there is evidence for infall motions on a large (~ 0.1 pc) scale in the double-peaked profiles of both optically thick CS lines and the likely optically thin $C^{34}S(2-1)$ transition (Lemme et al. 1995); the latter could come from an infalling shell, as in L1544 (Caselli et al. 1999). The optically thin tracer N_2H^+ shows, however, a single peaked spectrum (Lee, Myers & Tafalla 2001), indicating that it is centrally peaked, in contrast to $C^{34}S$. These similarities to L1544 point to a relatively advanced stage of pre-protostellar evolution for L1498, making it another valuable testing ground for chemical and dynamical models of (low-mass) star formation.

Common to both sources is the ring (or shell)-like structure of CCS, a well-known “early time” species (Bergin & Langer 1997) tracing chemically “young” material of order 10^5 yrs or less. This prominent feature should provide a strong constraint on models. Additional constraints should come from the inferred large CO depletion near the core center as well as the spatial extent and speed of the infall motions present in both L1544 and L1498. The question we want to address is: can the standard picture of dense core formation involving ambipolar diffusion satisfy these chemical *and* kinematic constraints simultaneously? A partial answer to this question has been provided by Bergin & Langer (1997), who considered the chemical evolution of a *parcel* of cloud material whose density increases with time in a prescribed way (i.e., a standard time dependent but depth independent model). They found that differential depletion of various molecular species onto dust grains must be a key ingredient in understanding the differentiated chemical structure

observed in L1498.

Aikawa et al. (2001) went one step further, and followed the evolution of molecular abundances of a dynamically collapsing starless core *as a whole*, with an emphasis on the spatial distribution. The study was based on the self-similar solution of Larson (1969) and Penston (1969) and its artificially delayed analogs. Among the dynamical models adopted, they found that the undelayed Larson-Penston model provides the best overall fit to the observational data on CO, CCS and N_2H^+ for L1544. If this result is robust, its implications would be far reaching. It is well known that the Larson-Penston solution describes the collapse of a cloud essentially on a free-fall time scale. The fact that it matches observations better than its delayed analogs appears to pose a serious challenge to the standard picture of star formation involving strongly magnetized cloud cores, which are formed through ambipolar diffusion on a time scale much longer than the free-fall time scale. However, the large infall velocity of the Larson-Penston solution, approaching 3.3 times the sound speed, is clearly incompatible with those inferred for L1544 and other starless cores, which are typically less than the sound speed (Lee et al. 2001). Furthermore, the best-fit model of Aikawa et al. under predicts the abundance of N_2H^+ by a large factor of ~ 20 . These discrepancies motivate us to reexamine the molecular evolution of starless cores using a more sophisticated dynamical model, one that is coupled to the cloud chemistry.

The dynamical model we will adopt is that of Li (1999). It is a spherical model of starless cores that takes into account the dynamic effects of magnetic field approximately. As envisioned in standard scenario of low-mass star formation, the cores in the model evolve through ambipolar diffusion, and their dynamics are coupled to chemistry through the abundances of charged species. Previously, we (Shematovich, Shustov, & Wiebe 1997; 1999) have modeled the chemistry of dynamically evolving clouds in detail. The chemical model will be combined with the dynamical model into a coupled dynamical-chemical model of magnetized starless cores. An advantage of the combined model is that it allows for a determination of not only the time evolution of various molecular species but also their *spatial* distributions *and* kinematics. We describe the formulation of the combined model in §2. In §3, we present representative model results, focusing on the density distribution, velocity field and abundance distributions of several commonly used molecular species. These results are compared with observations of L1544. We conclude and discuss our main results and future refinements in §4.

2. Formulation of Coupled Dynamical-Chemical Model

2.1. Dynamical Model

Ambipolar diffusion-driven evolution of strongly magnetized clouds has been modeled by many authors, although a complete understanding is still lacking. The numerical complexity of the problem forced most workers to adopt either a quasi-static approximation (e.g., Nakano 1979; Lizano & Shu 1989) or a simplified disk-like geometry (e.g., Basu & Mouschovias 1994; Ciolek &

Mouschovias 1994). Some 2D axisymmetric dynamical models are available (Fiedler & Mouschovias 1993; Desch & Mouschovias 2001), although incorporation of a full-blown chemical network into such models would be prohibitively expensive computationally at present. A simpler approach to the dynamical problem was pioneered by Safier, McKee & Stahler (1997). By retaining only the pressure component of the magnetic forces they were able to retain a spherical geometry, which simplifies the dynamics greatly. Indeed, they were able to obtain *analytic* solutions to both core formation and collapse assuming further that the thermal pressure is negligible and that the ions (and magnetic field lines tied to them) move much more slowly than neutrals. These last two assumptions have been relaxed in Li (1998) and the resulting set of governing equations can be solved efficiently, particularly in a Lagrangian form (Li 1999). The formulation of the dynamical problem by Li (1999) is employed in our coupled dynamical-chemical model.

For reference, we list below the equations governing the dynamic evolution of a spherical, magnetized cloud (taken from Li 1999) in dimensionless radius ζ , mass m , density $\hat{\rho}$, velocity u , magnetic field strength b and time τ :

$$\frac{\partial \zeta}{\partial m} = \frac{1}{\hat{\rho} \zeta^2}, \quad (1)$$

$$\frac{\partial u}{\partial \tau} = -\frac{m}{\zeta^2} - \zeta^2 \frac{\partial}{\partial m} \left(\frac{\hat{\rho}}{2\alpha_c} + \frac{b^2}{2} \right), \quad (2)$$

$$\frac{\partial}{\partial \tau} \left(\frac{b}{\hat{\rho} \zeta} \right) = \frac{\partial}{\partial m} \left(\frac{1.4 b^2 \zeta^2}{\nu_{\text{ff}} \hat{\rho}^{1/2}} \frac{\partial b}{\partial m} \right), \quad (3)$$

$$u = \frac{\partial \zeta}{\partial \tau}. \quad (4)$$

The density ρ and field strength B are scaled by their initial values at the cloud center ρ_c and B_c . The time t is measured in units of the initial free-fall time

$$t_{\text{ff},c} = \frac{1}{(4\pi G \rho_c)^{1/2}}, \quad (5)$$

at the cloud center, and the velocity V in units of the Alfvén speed

$$V_{\text{A},c} = \frac{B_c}{(4\pi \rho_c)^{1/2}}. \quad (6)$$

Scales for the radius r and mass M are then $r_c = V_{\text{A},c} t_{\text{ff},c}$ and $M_c = 4\pi \rho_c r_c^3$. There are two dimensionless quantities in the governing equations. The first, α_c , is the ratio of magnetic pressure to thermal pressure at the cloud center at $t = 0$. For simplicity, it will be taken to be unity, consistent with the current data on the magnetic fields in the interstellar clouds (Crutcher 1999). The second is the magnetic coupling parameter ν_{ff} defined as the ratio of the local free-fall time (at a given density ρ) to the magnetic field–neutral coupling time scale

$$\nu_{\text{ff}} = \frac{\gamma \rho_i}{\sqrt{4\pi G \rho}}, \quad (7)$$

where ρ_i is the total mass density of ions, and γ is an ion-neutral drag coefficient. An approximate value for the drag coefficient of $\gamma = 3.5 \times 10^{13} \text{ cm}^3 \text{ g}^{-1} \text{ s}^{-1}$ is given in Shu (1992), obtained assuming a mean molecular weight of ions of ~ 30 . We will adopt the above simple prescription for the coupling parameter in this initial study, although a more elaborate treatment taking into account of contributions from charged dust grains is possible (e.g., Nishi, Nakano & Umebayashi 1991; Li 1999) and will be implemented in the future.

2.2. Chemical Model

The chemical model used here has been described in detail by Shematovich et al. (1997, 1999). Here we summarize the main features briefly. We solve the equations of chemical kinetics describing reactions in interstellar clouds of relatively low density ($\sim 10^2 - 10^8 \text{ cm}^{-3}$) and temperature ($T \sim 10 - 100 \text{ K}$). Molecules are formed and destroyed both in gas-phase and on grain surfaces. The dust grains are supposed to be well mixed with gas and contain 1% of the cloud mass. We label different species, both neutral and charged, by $i = 0, 1, \dots, M$, with $i = 0$ denoting electrons. The evolving chemical composition is described through the number densities $n_i^g(r, t)$ in gas-phase and $n_i^d(r, t)$ on icy mantles. The exchange between gas and dust is driven by accretion and desorption processes. In general, the chemical abundances of all species are computed by integrating the equations

$$\frac{d}{dt}n_i^g(r, t) = \sum_j \sum_l K_{lj}^g n_l^g n_j^g - n_i^g \sum_j K_{ij}^g n_j^g - k_i^{\text{acc}} n_i^g + k_i^{\text{des}} n_i^d, \quad (8)$$

$$\frac{d}{dt}n_i^d(r, t) = \sum_j \sum_l K_{lj}^d n_l^d n_j^d - n_i^d \sum_j K_{ij}^d n_j^d + k_i^{\text{acc}} n_i^g - k_i^{\text{des}} n_i^d, \quad (9)$$

where K_{ij}^g and K_{ij}^d are the gas-phase and grain surface chemical reaction rates. The coefficients k_i^{acc} and k_i^{des} define the accretion and desorption rates for the i th component. These equations are integrated, along with the dynamical equations, at each point of the flow. The computed abundances are then used to determine the magnetic coupling parameter ν_{ff} , and to obtain column densities for various commonly used molecular tracers for comparison with observations.

2.2.1. Gas-Phase Reactions

We consider gas-phase reactions in the dense, dark regions of molecular clouds that are well shielded from the external UV radiation field. The reactions are initiated by galactic cosmic rays which ionize the most abundant species with an adopted rate of $1.3 \times 10^{-17} \text{ s}^{-1}$. The primary ions that are formed react quickly with abundant hydrogen and CO molecules, defining the main paths of chemical evolution.

We use the UMIST Rate95 file (Millar, Farquhar & Willacy 1997). The included elements are H, He, C, N, O, S, Si, Na, Mg, and Fe. Our chemical reaction network is mainly limited to those

species containing no more than two atoms of trace elements (i.e. all elements other than H and He), with a few exceptions. One of these exceptions is C₂S, which has been mapped interferometrically in L1498 (Kuiper et al. 1996), L1544 (Ohashi et al. 1999), and others. Its abundance and spatial distribution provide a crucial constraint on models, as discussed by Aikawa et al. (2001) and shown below. In total, our gas-phase network contains about 2000 reactions between 59 neutral and 83 ion species.

2.2.2. Grain Surface Reactions

The formation of icy mantles due to accretion and desorption has been taken into account. The accretion rate is given by

$$k_i^{\text{acc}} = \pi a^2 \langle v_i \rangle S_i n_{\text{gr}} s^{-1}, \quad (10)$$

where a and n_{gr} are the grain radius (taken to be 10^{-5} cm) and dust number density, $\langle v_i \rangle$ is the average thermal velocity of the species, and S_i the sticking probability. We assume $S_i = 0.3$ for all neutral species except H₂ and He (Willacy, Rawlings & Williams 1994). Two desorption mechanisms are included. They are thermal evaporation and cosmic ray induced impulsive thermal evaporation (Hasegawa & Herbst 1993). The dust temperature is assumed to be 7 K everywhere, close to the value inferred by Evans et al. (2001) and Zucconi, Galli & Walmsley (2001) near the center of L1544. The values of the sticking probability and desorption energies are uncertain. The sensitivity of our model to these uncertainties will be explored elsewhere.

After being accreted onto the grain surface, the species are allowed to react with one another mainly through the hydrogen addition reactions, with rates taken from Hasegawa, Herbst & Leung (1992). The surface products include saturated molecules (such as CH₄, H₂O and NH₃), homonuclear molecules (such as C₂, N₂, and O₂) and their hydrogenated forms, among others. The accretion limit to the surface hydrogen addition chemistry was taken into account through the first modification of rate equations proposed by Caselli, Hasegawa, & Herbst (1998). In addition to 53 surface reactions (including molecular hydrogen formation), we also consider the recombination of ions on grain surfaces. The products of dissociative recombination are assumed to return into the gas phase immediately. The effects of surface reactions on abundance distributions will be fully examined in a subsequent paper.

2.3. Initial and Boundary Conditions

We adopt as a starting point for our calculations an isolated molecular clump in mechanical equilibrium, with a magnetic pressure equal to the thermal pressure everywhere. The gas temperature is assumed to be 10 K and is kept constant throughout the computations. The initial molecular hydrogen central density is set to $n_{\text{H}_2} = 10^3 \text{ cm}^{-3}$ for all models. Without ambipolar diffusion, the cloud would remain in the equilibrium forever. At $t = 0$ ambipolar diffusion is switched on. The

cloud evolution is then followed numerically with reflection boundary conditions (i.e., zero spatial gradient) at the cloud center and with a free pressure boundary at the cloud outer edge.

The initial chemical composition is assumed to be mostly atomic. Species with non-zero initial abundances are listed in Table 1. Their abundances are given with respect to the number density of hydrogen nuclei. All hydrogen is assumed to be in a molecular form initially.

2.4. Numerical Method

We divide the computational domain into spatial zones of equal mass. At each time step, we first advance the chemical model to evaluate ion density ρ_i in each spatial zone. Equations (1), (2), and (4) are then solved to update the velocity, radius of zone boundary and density. A new distribution of magnetic field is obtained by solving the diffusion equation (3), with the magnetic coupling parameter calculated from the ion densities at the beginning of the time step.

The value of time step is computed from the usual magnetic Courant-Friedrich-Lewy condition to ensure dynamic stability. The chemical model is advanced over this time interval independently, with its own algorithm and smaller time substeps that are determined from the required abundance accuracy. We solve the chemical kinetics equations with the standard LSODE package, and terminate the computation when the central density reaches $n_{\text{H}_2} = 10^6 \text{ cm}^{-3}$. This density is close to the value inferred at the center of L1544. At higher densities the effects of charged dust grains on ν_{ff} may become dominant (Nishi et al. 1991), and such effects have not been taken into account in the current version of the code.

3. Representative Model Results

The initial conditions for forming starless cores are not well constrained, either observationally or theoretically. There is in principle a large parameter space to be explored. In this initial study, we will focus on two models that highlight the effects of magnetic field on the dynamics and chemistry. In the first model, we consider a standard, magnetic cloud with a mass of $20 M_{\odot}$ (StM+B). The second model is identical to the first except that the magnetic field strength is set to zero (i.e., non-magnetic; StM–B). For reference, we also consider the dynamics of a model that is the same as the first except that the magnetic coupling parameter is fixed at the canonical value of $\nu_{\text{ff}} = 10$ instead of being computed self-consistently. These models are summarized in Table 2.

3.1. Dynamics

The main dynamic quantities of the models (density distribution and velocity field) are displayed in Figs. 1–3, along with the ionization fraction and magnetic coupling parameter for the

StM+B model. As mentioned earlier, all models start with a central density of $n_{\text{H}_2} = 10^3 \text{ cm}^{-3}$, typical of clouds in transition from being diffuse to dark. Note that when a certain center density is reached, the difference in density profile is modest, with that in the non-magnetic model somewhat peakier than those in the magnetic models. The difference in the time it takes to reach a given density is more pronounced. In Table 3 we list the time intervals taken to increase the central density by successive factors of 10. The time for the first factor-of-10 increase, to a value of 10^4 cm^{-3} characteristic of dense molecular cores, is $\sim 1 \text{ Myr}$ for the non-magnetic model. It is substantially shorter than those for the magnetic models ($\sim 4 - 5 \text{ Myrs}$). The times for subsequent 10-fold increases become shorter and shorter, and the differences in time between the models also get smaller. The time for the second (and third) factor-of-10 increase is longer for the magnetic models than for the non-magnetic one by only a factor of ~ 2.5 (and ~ 2). In other words, after formation a magnetic starless *dense core* typically lasts for only a few free-fall times before stellar birth. *That the evolutionary time scale becomes closer to that of a non-magnetic, free-falling model at higher densities is an important feature of the ambipolar diffusion-driven cloud evolution. This characteristic cannot be captured by simply adding a constant delay factor to a non-magnetic model,* as done for example in Aikawa et al. (2001). The differences in time scale among the models will have a decisive influence on the chemistry, with potentially observable consequences.

Another potentially observable difference among the models is the velocity field. From Figs. 1–3 we find that the infall speed is typically a few tenths of 1 km s^{-1} , comparable to the isothermal sound speed of the cloud ($a = 0.188 \text{ km s}^{-1}$ at 10 K). As expected, the non-magnetic model collapses right away, approaching a maximum speed ~ 2.3 times larger than the sound speed a by the time of a 10^3 -fold increase in the central density. Even this maximum speed is substantially lower than that in a Larson-Penston flow, which is 3.3 times the sound speed. The infall speed in magnetized models increases more gradually, reaching a *maximum* value of $\sim 0.35 \text{ km s}^{-1}$ (or about twice the sound speed) for the StM+B and reference model when the central density reaches $n_{\text{H}_2} = 10^6 \text{ cm}^{-3}$, roughly the density inferred for the central region of L1544 (Ward-Thompson et al. 1999). Note that the density distribution flattens near the center for all three models, more so in the magnetic models than in the non-magnetic one. The radius of the central flat region is of order $\sim 2 - 3 \times 10^3 \text{ AU}$ for the StM+B model, consistent with those deduced by Ward-Thompson et al. (1999) and Bacmann et al. (2000). The predicted peak H_2 column density of $\sim 10^{23} \text{ cm}^{-2}$ also agrees with the value inferred by Ward-Thompson et al. (1999) within a radius of $\sim 900 \text{ AU}$. However, the observationally inferred infall velocity for L1544 of order 0.1 km s^{-1} (Tafalla et al. 1998; Williams et al. 1999; Ohashi et al. 1999) is lower than predicted. The discrepancy, although substantial, is less severe in our model than in those of Aikawa et al. (2001). It could be further reduced by taking into account the projection effects in a more realistic flattened geometry and the effects of magnetic tension on cloud dynamics (Ciolek & Basu 2000).

Table 1: Species with Non-Zero Initial Abundances

Species	Abundance
H ₂	0.5
He	0.1
Na	2.1(−6)
Mg	1.5(−7)
Fe	1.0(−7)
C	1.0(−5)
N	2.2(−5)
O	1.3(−4)
CO	4.0(−5)
S	8.0(−8)
Si	8.0(−9)

Table 2: Model Summary

Model Name	ν_{ff}	Magnetic Field
Reference	fixed at 10	yes
StM+B	variable	yes
StM−B	not relevant	no

Table 3: Time Intervals (in Myrs) for Central Density Increase

H ₂ density (cm ^{−3})	Reference Model	StM+B	StM−B
10 ³ –10 ⁴	4.35	5.05	1.32
10 ⁴ –10 ⁵	0.47	0.53	0.19
10 ⁵ –10 ⁶	0.10	0.11	0.05

3.2. Ionization Fraction and Magnetic Coupling Parameter

Before showing results on chemical abundances, we comment on the ionization fraction x_i (defined as the ratio of the number density of all ions to that of hydrogen nuclei) and magnetic coupling parameter ν_{ff} , both of which are shown in Fig. 2 for the StM+B model. The fraction x_i decreases with density, as expected. Its lowest value of $\sim 3 \times 10^{-9}$ at the center of the cloud is somewhat higher than that inferred for L1544 by Caselli et al. (2001b), although the inference is model dependent. The ionization fraction yields a magnetic coupling parameter ν_{ff} within a factor of two of the canonical value of 10.

3.3. Chemical Abundances and Comparison with L1544

3.3.1. Observationally Inferred Abundances in L1544

We concentrate on the abundances of six species, including CO, CS, CCS, HCO⁺, NH₃ and N₂H⁺. Other species will be considered in a subsequent paper of the series. For CO, CCS, HCO⁺, and N₂H⁺, the column density distributions have been inferred from observations in L1544. Caselli et al. (2001b) found that CO is heavily depleted near the center of L1544, by a factor up to ~ 10 . Its column density distribution is flat or slightly depressed near the center, with an average central value of $\sim 1.5 \times 10^{18} \text{ cm}^{-2}$, although large scatter exists in the data (see their Fig. 5). Both HCO⁺ and N₂H⁺ are centrally peaked, with a peak column density of $\sim 10^{14}$ and $\sim 2 \times 10^{13} \text{ cm}^{-2}$ respectively. Ohashi et al. (1999) mapped L1544 interferometrically in CCS. They found that CCS peaks in a ring of radius $\sim 7,500 \text{ AU}$. The peak CCS column density is $\sim 4 \times 10^{13} \text{ cm}^{-2}$, which is ~ 1.4 times higher than the value at the center (Aikawa et al. 2001). Observational data on NH₃ and CS appear to be less complete. Using the Nobeyama 45 m telescope, Suzuki et al. (1992) observed L1544 in NH₃ and derived an average column density of $2.7 \times 10^{14} \text{ cm}^{-2}$ within a region of radius $\sim 6,000 \text{ AU}$, corresponding to a beamwidth of $80''$. L1544 has been observed in CS (Tafalla et al. 1998), although the peak value and spatial distribution of its column density are not yet available.

3.3.2. Standard Magnetic Model

The column density distributions of the six species of interest for the StM+B model, obtained by integrating the number densities along the line of sight at various distances from line of sight through the cloud center, are shown in Fig. 4. We will concentrate on the last time ($t=5.69 \text{ Myrs}$) when the density distribution fits approximately that observed (Ward-Thompson et al. 1999). It is immediately evident from the figure that a central hole exists in the distribution of CCS, with a radius ($\sim 7,000 \text{ AU}$) and depth (~ 1.3) that match almost exactly those observed (Ohashi et al. 1999). Note the differentiated chemical structure, with the centrally peaked NH₃ and N₂H⁺

surrounded by a CCS ring, which is in turn embedded within a slightly broader CS ring². The predicted peak column density for N_2H^+ of $1.3 \times 10^{13} \text{ cm}^{-2}$ is within a factor of 2 of the observed value ($\sim 2 \times 10^{13} \text{ cm}^{-2}$). The predicted peak column density for NH_3 of $5.5 \times 10^{14} \text{ cm}^{-2}$ is about twice the value $2.7 \times 10^{14} \text{ cm}^{-2}$ given by Suzuki et al. (1992). Averaging the column density over a radius of 6,000 AU (the beamwidth) yields a value $\sim 2 \times 10^{14} \text{ cm}^{-2}$, which is in a closer agreement with Suzuki et al.’s value. From Fig. 4 we see that HCO^+ is also centrally peaked, although less sharply than N_2H^+ , again in agreement with observation (see Fig. 5 of Caselli et al. 2001b). Its predicted peak column density of $4.5 \times 10^{13} \text{ cm}^{-2}$ is about a factor of two lower than observed ($\sim 10^{14} \text{ cm}^{-2}$). The CO column density in this model shows a relatively flat distribution near the center, with a maximum value of $1.6 \times 10^{18} \text{ cm}^{-2}$, almost identical to the observed value. Its spatial distribution appears to be consistent with that inferred by Caselli et al. (2001b) within errors. The model predicts that the column density distribution of CS should have a shallow depression near the center. Data for testing this prediction are not yet available. We conclude that, within a factor of two or so, the predictions of the StM+B model on the abundances of CO, N_2H^+ , HCO^+ and NH_3 are consistent with the data available on L1544.

The abundance and spatial distribution of CCS deserve special attention. We have mentioned the close fit to the observed spatial distribution and will now concentrate on abundance. The CCS molecule is a well-known “early time” species. Its abundance should decrease, according to Bergin & Langer (1997), rapidly after a few times 10^5 years, as a result of neutral atomic carbon being converted into CO (see also Suzuki et al. 1992 and Aikawa et al. 2001). One might expect to find little CCS in the magnetic cloud of the StM+B model, which reaches the observed state after nearly 6 million years of evolution. However, this turns out not to be the case, as shown in Fig. 4. The predicted peak CCS column density is $1.3 \times 10^{13} \text{ cm}^{-2}$, about a third of the observed value ($\sim 4 \times 10^{13} \text{ cm}^{-2}$). The agreement would be closer, if one takes into account of likely projection effects. The CCS ring is seen almost edge-on, judging from its large aspect ratio (~ 3 ; Ohashi et al. 1999). The nearly edge-on geometry implies a smaller peak column density *perpendicular to the ring*, by a factor of ~ 3 . It turns out that CCS plays a crucial role in discriminating models. We will postpone a more detailed discussion of this molecule to § 4.1. Here, we simply note that the StM+B model appears to reproduce all abundance data on L1544 reasonably well. It is the “standard” model against which other models will be compared.

3.3.3. Free-Falling Non-Magnetic Model

Without magnetic support, the cloud considered in the previous subsection collapses promptly, reaching the observed state in 1.56 million years. This faster dynamic evolution affects the chemical

²This is not exactly what is observed in L1498, where CS appears to concentrate near the inner edge of the CCS ring (Kuiper et al. 1996). The situation with L1544 is unclear, although there is some indication that a central hole exists in CS as well (Tafalla 2001; priv. comm.).

abundances, as shown in Fig. 5. The effects on CO, NH₃, N₂H⁺ and HCO⁺ are relatively modest. The peak column density of CO differs little from that of the standard model. Its spatial distribution appears more centrally peaked, however, which is more difficult to reconcile with observation. The distributions of N₂H⁺, NH₃ and HCO⁺ are centrally peaked, as in the standard model. Compared with the standard model, the peak value for N₂H⁺ is down by a factor of ~ 2 , making it significantly below the observed value (by a factor of ~ 4). The column density of NH₃ is also down by a similar factor of ~ 2 , making the fit to the value inferred by Suzuki et al. (1992) worse. The column density of HCO⁺ is lower by a modest factor of $\sim 20\%$.

The difference in CS and CCS is more pronounced. Unlike in the standard model, the column density distributions of CS and CCS in the non-magnetic model are centrally peaked instead of showing a central depression. While the observational situation with CS is still unclear at present, a central peak in CCS is definitively ruled out. One potentially desirable feature of the non-magnetic model is that the peak column density of CCS is about twice the value in the standard model, making it closer to the observationally inferred value without projection corrections. However, its overall fit to all available data is significantly worse than that of the standard model. This result lends some support the standard picture of low-mass star formation involving core formation through ambipolar diffusion over a time scale substantially longer than free fall. The peak value and spatial distribution of the column density of CS would further constrain the models but are not yet available. They are urgently needed.

We note that our non-magnetic model is similar to the undelayed model of Aikawa et al. (2001), except that we have included some surface reactions and adopted a smaller sticking probability.

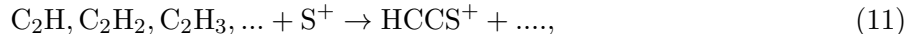
4. Discussion and Conclusions

4.1. Magnetic Cloud Support and CCS Abundance

The success of the standard, magnetic model in fitting the data on L1544 hinges to a large extent on the relatively high abundance predicted for CCS. This result is somewhat surprising in view of the fact that CCS is a well-known “early time” species, whose abundance should decline rapidly after a few times 10^5 years according to Suzuki et al. (1992), Bergin & Langer (1997), and Aikawa et al. (2001). Part of the reason for the persistently high CCS abundance in the standard model even after some 5.69 Myrs of evolution (the time it takes the cloud to reach the observed state) is that we adopted an initial cloud density of $n_{\text{H}_2} = 10^3 \text{ cm}^{-3}$, which is lower than those of Bergin & Langer ($10^{3.5} \text{ cm}^{-3}$) or Suzuki et al. and Aikawa et al. (10^4 cm^{-3}). As a result, the bulk of the 5.69 Myrs is spent in the “pre-dense core” phase when the central density remains below 10^4 cm^{-3} (see Table 3). Only a small fraction ($\sim 10\%$) of that time is spent at densities above 10^4 cm^{-3} . That a cloud spends a relatively short time (a few times the free-fall time) at high densities after forming a magnetically supercritical core is a general feature of ambipolar diffusion-driven evolution. It helps to keep the CCS abundance higher than one would expect based on the

total time of cloud evolution.

The fractional abundances of CCS are shown in Fig. 6 as a function of radius for both the magnetic and non-magnetic models. Note the “humps” on the distributions of CCS abundance in the magnetic model, which are not apparent in the non-magnetic model. The exact origin of the humps is unclear. We suspect that they are related to the depletion of CO in the central high density region, similar to the “depletion” peak proposed by Ruffle et al. (1997) for HC₃N. Ruffle et al. (1997, 1999) showed that C₂H and HC₃N in dense, cold cores are characterized by a secondary “late-time” maximum in their fractional abundances. The second peak is thought to be mainly caused by the increased depletion of CO, which allows C⁺ ion to react more readily with H₂ than with oxygen bearing species. The net result is an increase in the rates of production of CH and other carbon-bearing molecules (without oxygen). It was found that high late-time C₂H and HC₃N maxima are achieved only when the freeze-out time scale is long compared to the chemical time scale. Because C₂H and other (neutral and ionized) late-time hydrocarbons are the precursors of CCS formation in the reactions with neutral and ionized sulfur through



CCS should behave in a way similar to the C₂H and HC₃N. The competition between depletion and late-time hydrocarbon chemistry enhanced by CO-depletion appears to be the most likely cause of the humps on the radial profiles of CCS abundance.

In any case, the humps have apparently kept the CCS abundance of the magnetic model close to, and in some regions exceeding, that of the non-magnetic model. They are largely responsible for the higher-than-expected value of the CCS column density in the magnetic model. In addition, the decline of CCS abundance outside the hump, coupled with a steep decrease in the hydrogen number density with radius, may explain the observed rapid decline of the CCS column density outside the ring (Ohashi 2001; priv. comm.).

4.2. Depletion of Molecules onto Dust Grains

4.2.1. Depletion of CO and Other Species

In the standard model, CO is heavily depleted in the central high density region. The depletion is most clearly seen in the first panel of Fig. 7, where the fractional abundance is plotted as a function of radius. The abundance is significantly below the canonical value of 4.7×10^{-5} inside a radius of $\sim 10^4$ AU, by a factor up to ~ 30 . The size of the depletion region is roughly consistent with that deduced by Caselli et al. (2001b; their Fig. 2). The depletion is less evident in the CO column density distribution (see Fig. 4), which is flat near the center. The ratio of CO and hydrogen in

peak column density is a factor of ~ 5 below the canonical value. This depletion factor is about half of the value (~ 9) inferred by Caselli et al. (2001b). Their inference is based on the observations of $C^{17}O$, $C^{18}O$, and dust emission (Ward-Thompson et al. 1999). In particular, an dust opacity of $0.005 \text{ cm}^2\text{g}^{-1}$ was adopted to convert the dust continuum flux into a hydrogen column density. At densities as high as 10^6 cm^{-3} , an opacity of $\sim 0.01 \text{ cm}^2\text{g}^{-1}$ may be more appropriate (Ossenkopf & Henning 1994), which would lower the estimate of the hydrogen column density by half and bring a closer agreement between the model prediction and observation. Alternatively, a flattened geometry, as observed for L1544, and/or a somewhat higher CO adsorption energy (see Aikawa et al. 2001) may enhance the CO depletion in the column density distribution.

Besides CO, there are other species that are strongly depleted in the high density central region. These include CS, CCS and to a lesser extent HCO^+ , as can be seen from Fig. 7. The nitrogen bearing species, N_2H^+ and NH_3 , are on the other hand hardly depleted; if anything, their abundances are slightly enhanced near the center. This differential depletion pattern is in agreement with previous findings (e.g., Bergin & Langer 1997; Aikawa et al. 2001). It may have profound effects on the molecular line profiles used to probe cloud kinematics.

4.2.2. *Effects of Depletion on Line Profiles*

An interesting observational fact about L1544 is that some optically thin lines in L1544, such as CCS (Ohashi et al. 1999) and $HC^{18}O^+$ (Caselli et al. 2001b), are double-peaked. As noted by Caselli et al. (1999, 2001b), the double-peaked optically thin lines can be explained in a collapsing cloud *provided* that the line-emitting molecules are strongly depleted near the center. We have seen from Fig. 7 that CCS and, to a lesser extent, HCO^+ (and thus $HC^{18}O^+$) are indeed centrally depleted in our standard model. A unique strength of the coupled dynamical-chemical model is that it allows for a simultaneous determination of the spatial distribution of a given species and the velocity field, the two ingredients for line profile modeling. In a subsequent paper, we will produce synthetic line profiles for both optically thin and thick lines (such as CS and HCO^+ ; Tafalla et al. 1998), which should enable us to constrain the models of core formation leading to star formation using both the spatial *and* kinematic information of molecular species.

4.3. Conclusions

We have developed a coupled dynamical and chemical model for the starless cores of strongly magnetized molecular clouds. The coupling is achieved through ions, the abundances of which are determined self-consistently from a chemical network. The ionic abundances control the time scale of cloud dynamic evolution via ambipolar diffusion. We have concentrated on a representative model in which an isolated magnetic cloud increases its central number density by a factor of 10^3 to $n_{H_2} = 10^6 \text{ cm}^{-3}$ in 5.69 million years, with an eye on explaining the observational data on the

chemical abundances of the well-studied starless core L1544. We find that the predicted peak values of CO, CCS, N_2H^+ and HCO^+ column densities are within a factor of two or so of those inferred for L1544 from observations. The spatial distributions of these species are also consistent with those observed. An alternative, non-magnetic model was also considered for comparison. With the same initial conditions as in the magnetic model, the non-magnetic cloud collapses promptly, reaching the observed state in merely 1.56 million years. It produces a worse overall fit to the available data on L1544. In particular, the column density distribution of CCS predicted by the model is centrally peaked, which is not observed.

We conclude that our initial results of modeling lend some support to the standard picture of dense core formation out of strongly magnetized molecular clouds involving ambipolar diffusion over several dynamic times. There are, however, a number of uncertainties to which the results may be sensitive to, including the sticking probability and adsorption energies for various species. A parameter survey is needed to firm up the conclusion.

4.4. Future Refinements

There are several aspects of the coupled model that we wish to improve upon in the future. These include both dynamics and chemistry. Even though our spherical model captures the essence of the ambipolar diffusion-driven cloud evolution, the effects of magnetic tension (which tend to flatten a cloud) cannot be treated. Indeed, the opposite extreme, a disk-like geometry, may describe the observed elongated mass distribution in L1544 better. It should be straightforward to extend the model to this geometry, which would allow for the inclusion of rotation whose presence has been inferred for L1544 by Ohashi et al. (1999) based on CCS data. On the chemistry side, a major uncertainty is the adsorption energies for CO and other species. Different sets of adsorption energies have been considered by Aikawa et al. (2001), and a similar parameter study is needed for our model. Also uncertain are the probability of molecules sticking onto dust grains and grain surface processes, and an exploration of different cases is desirable. Another area of improvement would be the treatment of magnetic coupling coefficient, by including the effects of charged dust grains (especially small ones) and external UV radiation field.

The authors are grateful to P. Murphy and B. Turner for access to NRAO computing facilities, and to P. Caselli and the referee for helpful comments. This research is supported in part by RFBR Grant 01-02-16206.

REFERENCES

Aikawa, Y., Ohashi, N., Inutsuka, S., Herbst, E., & Takakuwa, S. 2001, *ApJ*, 552, 639

- Bacmann, A., Andre, P., Puget, J.-L., Abergel, A., Bontemps, S., Ward-Thompson, D. 2000, AA, 361, 555
- Basu, S., Mouschovias, T. Ch. 1994, ApJ, 432, 720
- Beichman, C. A., Myers, P. C., Emerson, J. P., Harris, S., Mathieu, R., Benson, P. J., & Jennings, R. E. 1986, ApJ, 307, 337
- Bergin, E. A., & Langer, W. D. 1997, ApJ, 486, 316
- Caselli, P., Hasegawa T.I. & Herbst, E. 1998, ApJ, 495, 309
- Caselli, P., Walmsley, C. M., Tafalla, M., Dore, L., & Myers, P. C. 1999, ApJ, 523, L165
- Caselli, P., Walmsley, C. M., Tafalla, M., Dore, L., & Myers, P. C. 2001a, ApJ, in press
- Caselli, P., Walmsley, C. M., Tafalla, M., Dore, L., & Myers, P. C. 2001b, ApJ, in press
- Ciolek, G. E. & Basu, S. 2000, ApJ, 529, 925
- Ciolek, G. E. & Mouschovias, T. Ch. 1994, ApJ, 425, 142
- Crutcher, R. M. 1999, ApJ, 520, 706
- Crutcher, R. M. & Troland, T. H. 2000, ApJ, 537, L139
- Desch, S. J., & Mouschovias, T. 2001, ApJ, 550, 314
- Elias, J. H. 1978, ApJ, 224, 857
- Evans, N. J., Rawlings, J. M. C., Shirley, Y. L., & Mundy, L. G. 2001, ApJ, 557, 193
- Fiedler, R. A. & Mouschovias, T. Ch. 1993, ApJ, 415, 680
- Hasegawa, T.I., Herbst, E., & Leung, C.M. 1992, ApJS, 82, 405
- Hasegawa, T.I., & Herbst, E. 1993, MNRAS, 261, 83
- Kuiper, T. B. H., Langer, W. D., & Velusamy, T. 1996, ApJ, 468, 761
- Larson, R. B. 1969, MNRAS, 145, 271
- Lee, C.-W., Myers, P. C. & Tafalla, M. 2001, ApJ, in press (astro-ph/0105515)
- Lemme, C., Walmsley, C. M., Wilson, T. L. & Muders, D. 1995, AA, 302, 509
- Li, Z.-Y. 1998, ApJ, 493, 230
- 1999, ApJ, 526, 806

- Lizano, S. & Shu, F. H. 1989, *ApJ*, 342, 834
- Millar, T.J., Farquhar, P.R.A., & Willacy, K. 1997, *Astron. Astrophys. Suppl.*, 121, 139
- Myers, P. C. 1999, in *The Origins of Stars and Planetary Systems*, eds. C. Lada & N. Kylafis (Dordrecht: Kluwer), p67
- Nakano, T. 1979, *PASJ*, 31, 697
- Nishi, R., Nakano, T. & Umebayashi, T. 1991, *ApJ*, 368, 181
- Ohashi, N., Lee, S. W., Wilner, D. J., & Hayashi, M. 1999, *ApJ*, 518, L41
- Penston, M. V. 1969, *MNRAS*, 144, 425
- Ruffle, D. P., Hartquist, T. W., Taylor, S. D., & Williams, D. A. 1997, *MNRAS*, 291, 235
- Ruffle, D. P., Hartquist, T. W., Caselli, P., & Williams, D. A. 1999, *MNRAS*, 306, 691
- Safier, P. N., McKee, C. F. & Stahler, S. W. 1997, *ApJ*, 485, 660
- Shematovich, V.I., Shustov, B.M., & Wiebe, D.S. 1997, *MNRAS*, 292, 601
- Shematovich, V.I., Shustov, B.M., & Wiebe, D.S. 1999, *Astron. Reports*, 43, 645
- Shu, F. H. 1992, *The Physics of Astrophysics II* (Mill Valley: University Science Books)
- Shu, F. H., Allen, A., Shang, H., Ostriker, E. & Li, Z.-Y. 1999, in *The Origins of Stars and Planetary Systems*, eds. C. Lada & N. Kylafis (Dordrecht: Kluwer), p193
- Shu, F. H., Adams, F. C. & Lizano, S. 1987, *ARAA*, 25, 23
- Suzuki, H., Yamamoto, S., Ohishi, M., et al. 1992, *ApJ*, 392, 551
- Taffala, M., Mardones, D., et al. 1998, *ApJ*, 504, 900
- Ward-Thompson, D., Motte, F. & Andre, P. 1999, *MNRAS*, 305, 143
- Ward-Thompson, D., Kirk, J. M., Crutcher, R. M., et al. 2000, *ApJ*, 537, L135
- Willacy, K., Langer, W.D., & Velusamy, T. 1998, *ApJ*, 507, L171
- Willacy, K., Rawlings, J.M.C., & Williams, D.A. 1994, *MNRAS*, 269, 921
- Williams, J. P., Myers, P. C., Wilner, D. J. & di Francesco, J. 1999, *ApJ*, 613, L61
- Zucconi, A., Walmsley, C. M. & Galli, D. 2001, *AA*, in press

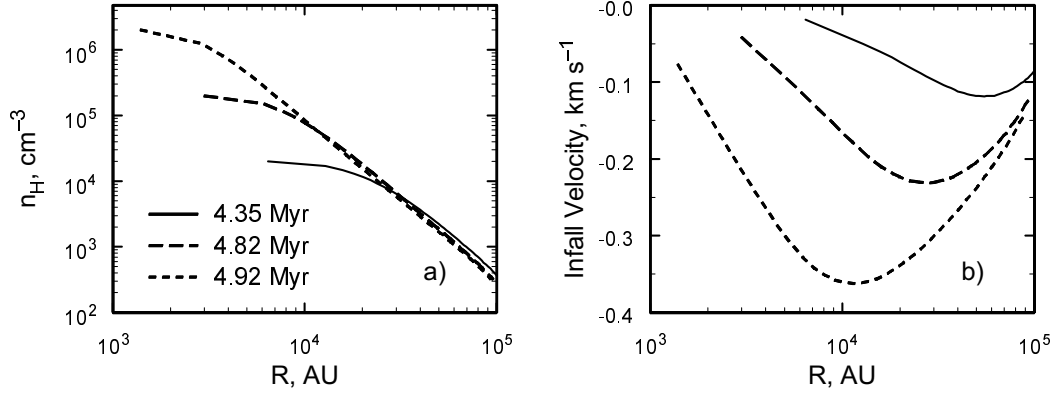


Fig. 1.— Radial profiles of the number density of hydrogen nuclei (a) and infall velocity (b) for the reference model at three times when the central density reaches 10, 10^2 and 10^3 times its initial value respectively.

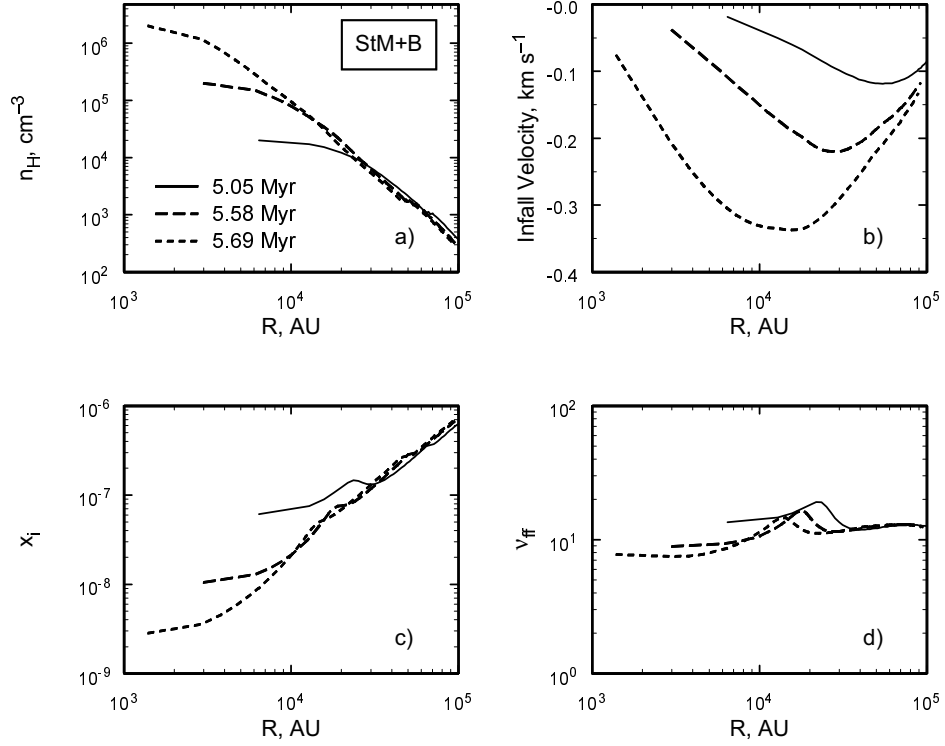


Fig. 2.— Radial profiles of the number density of hydrogen nuclei (a), infall velocity (b), ionization fraction (c), and magnetic coupling parameter (d) for the standard, magnetic model.

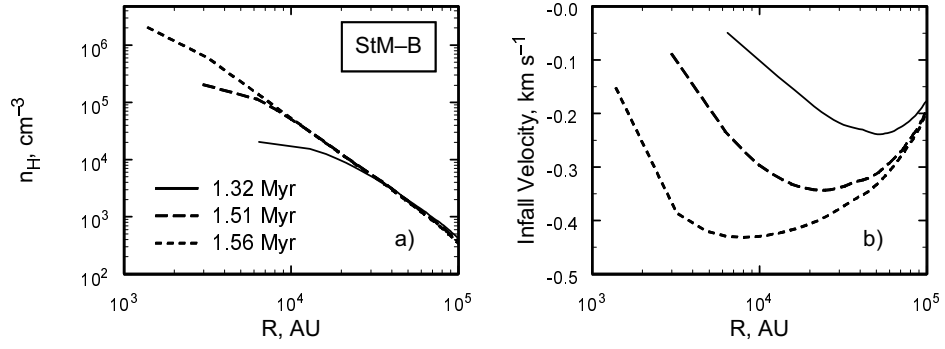


Fig. 3.— Radial profiles of the number density of hydrogen nuclei (a) and infall velocity (b) for the non-magnetic model.

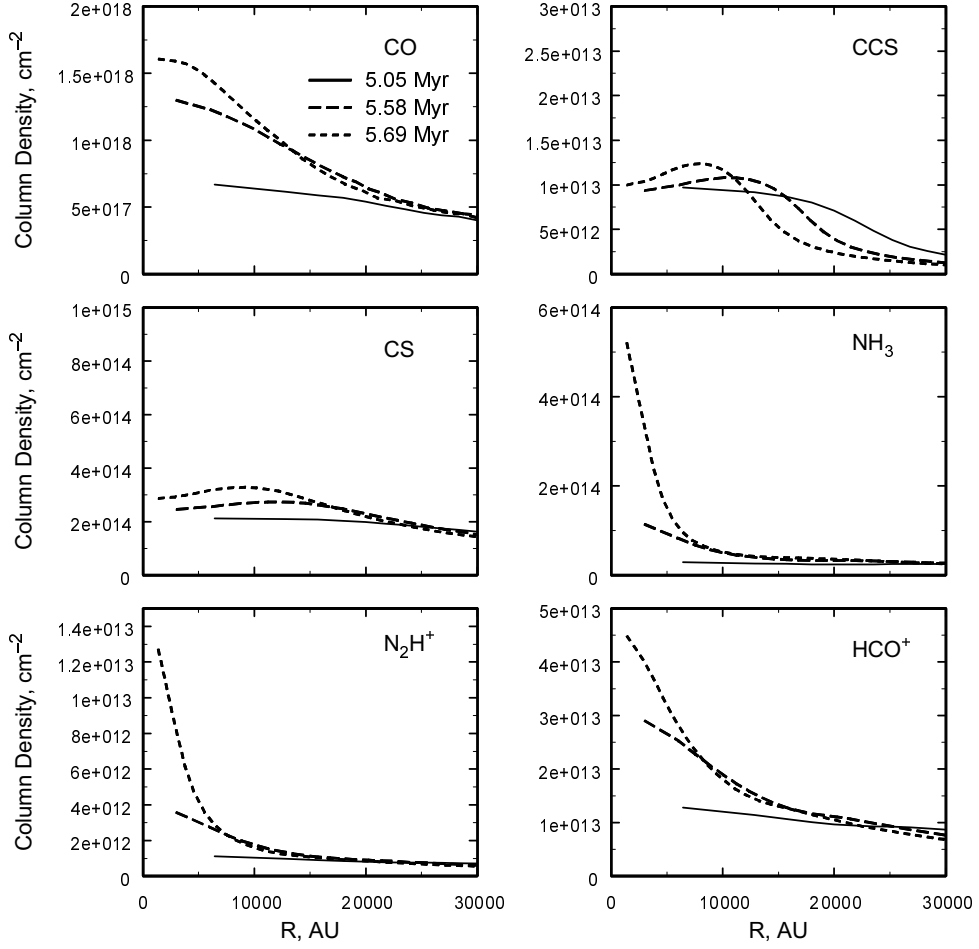


Fig. 4.— Column density distributions of CO, CCS, CS, NH₃, N₂H⁺, and HCO⁺ for the standard, magnetic model.

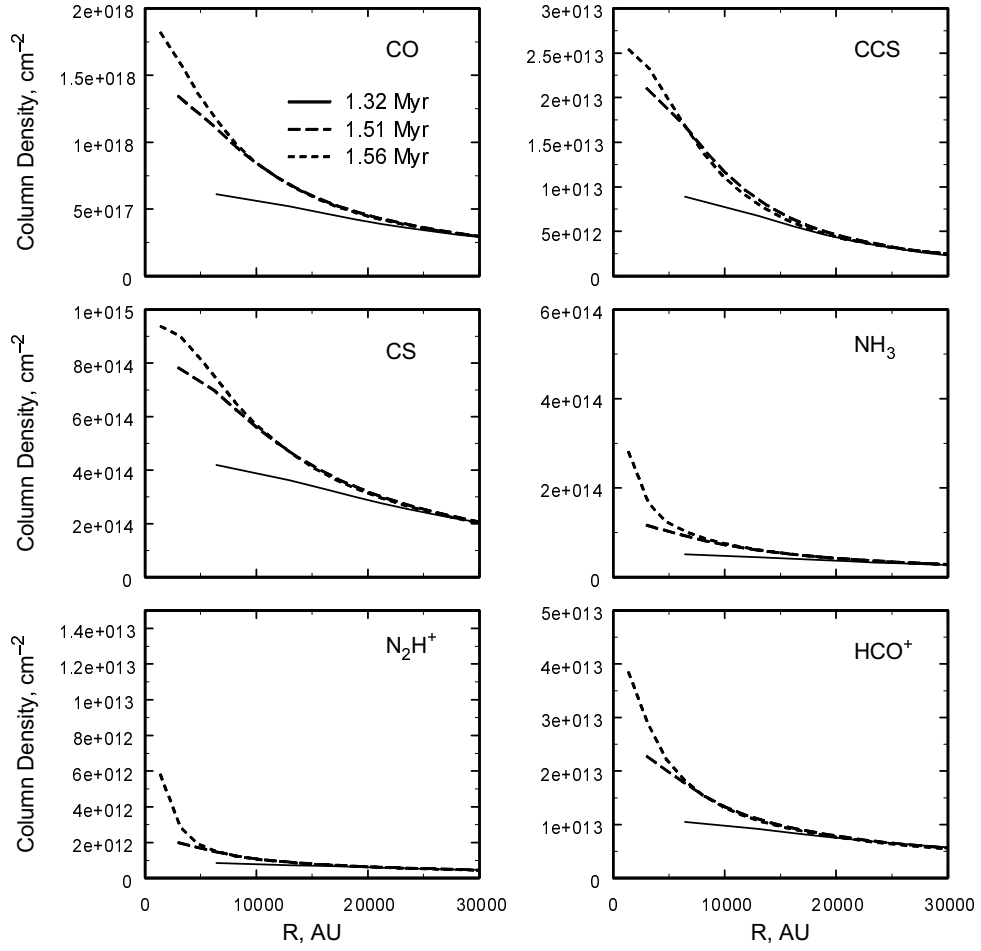


Fig. 5.— Column density distributions of CO, CCS, CS, NH₃, N₂H⁺, and HCO⁺ for the non-magnetic model.

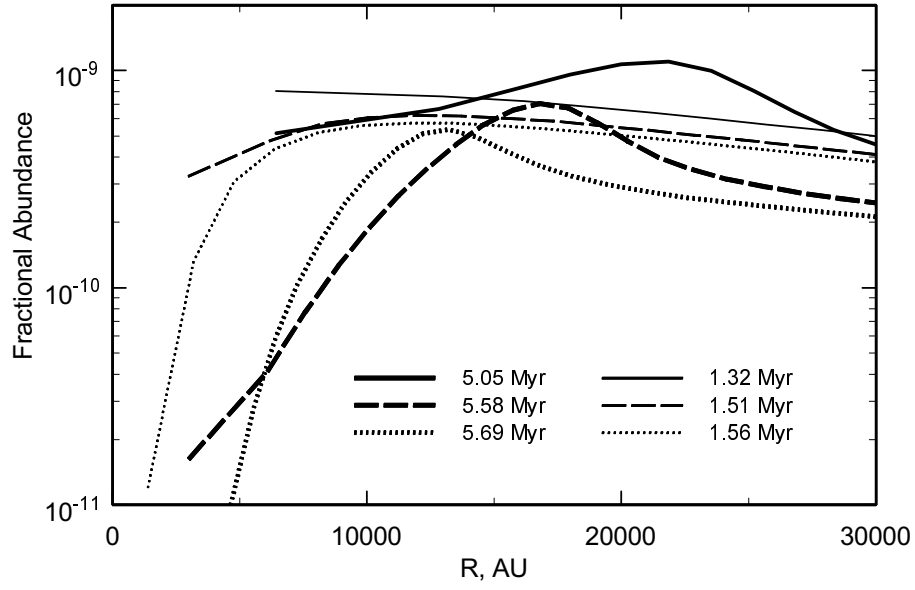


Fig. 6.— Radial profiles of the fractional abundances of CCS for both the magnetic (heavy lines) and non-magnetic (light lines) models.

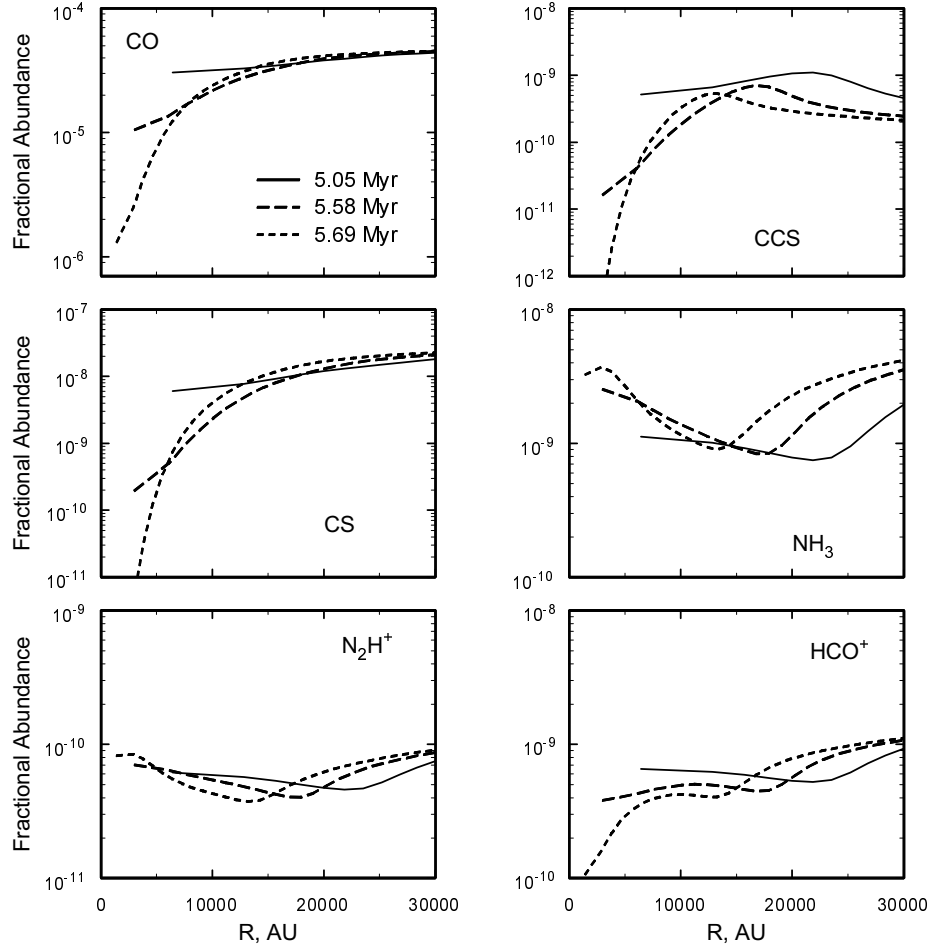


Fig. 7.— Radial profiles of the fractional abundances of CO, CCS, CS, NH₃, N₂H⁺, and HCO⁺ for the standard, magnetic model.